THE JOURNAL OF PHYSICAL CHEMISTRY B

Article

pubs.acs.org/JPCB

Binding of the Antitubercular Pro-Drug Isoniazid in the Heme Access Channel of Catalase-Peroxidase (KatG). A Combined Structural and Metadynamics Investigation

Pietro Vidossich,[○,†] Peter C. Loewen,[○,‡] Xavi Carpena,[§] Giacomo Fiorin,[∥] Ignacio Fita,[⊥] and Carme Rovira*[,@,▽]

[†]Unitat de Química Física, Departament de Química, Universitat Autònoma de Barcelona, 08193 Bellaterra, Spain

[‡]Department of Microbiology, University of Manitoba, Winnipeg, MB R3T 2N2, Canada

[§]IRB Barcelona, Parc Científic de Barcelona, Baldiri Reixac 10-12, 08028 Barcelona, Spain

[∥]Institute for Computational Molecular Science, Temple University, 1900 N. 12th Street, Philadelphia, PA 19122, United States

[⊥]Institut de Biologia Molecular (IBMB-CSIC), Parc Científic de Barcelona, Baldiri Reixac 10-12, 08028 Barcelona, Spain

[@]Institució Catalana de Recerca i Estudis Avançats (ICREA), Passeig Lluís Companys, 23, 08018 Barcelona, Spain

[▽]Departament de Química Orgànica and Institut de Química Teòrica i Computacional (IQTCUB), Universitat de Barcelona, Diagonal 645, 08028 Barcelona, Spain

Supporting Information

ABSTRACT: Isonicotinic acid hydrazide (isoniazid or INH) is a front line antitubercular pro-drug that is converted to its active form, isonicotinyl-NAD, by the bacterial catalase-peroxidase KatG. Understanding the role of KatG in the INH activation process has been hampered by a lack of knowledge of the actual drug binding site. In this work, we have investigated the binding of INH in the main access channel of KatG with a combination of molecular dynamics, using an enhanced-sampling technique (metadynamics), X-ray crystallography, and site-directed mutagenesis. The metadynamics simulations show that there are several weak drug binding sites along the access channel. Moreover, the simulations evidence that complete entrance to the heme active site is impeded by an aspartate residue (D141) located above the heme. This has been confirmed by structural and functional analysis of the D141A mutant, leading to the first X-ray crystallography evidence of INH at the heme access channel.

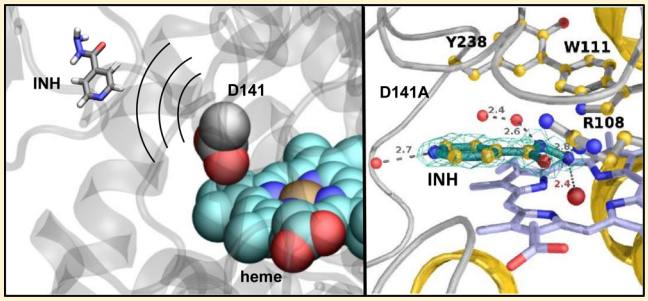

INTRODUCTION

Isonicotinic acid hydrazide (isoniazid or INH, Figure 1a) is a front line antitubercular pro-drug that is activated by the catalase-peroxidase (KatG) of *Mycobacterium tuberculosis* (MtKatG) (Figure 1b).[1−3] The central role of KatG in INH activation has been well-characterized in the identification of a large number of KatG mutants that impart INH resistance to the bacterium.[4−7] A serine located in the heme access channel is the most abundant site of mutations imparting INH resistance.[8,9]

Activation of INH involves cleavage to form an isonicotinyl radical that couples with NAD^+ to form isonicotinyl-NAD (IN-NAD),[10] which binds to and inhibits an enoyl−acyl carrier protein reductase (InhA) that is essential for mycolic acid synthesis and growth of the bacterium.[11,12]

The significant nonenzymatic rate of IN-NAD formation, which is enhanced only 6-fold by KatG,[13] suggests that KatG has relatively weak affinity for INH.[13] However, slowing the rate of IN-NAD synthesis to 1/3 in the S315T mutant is sufficient to impart INH resistance.

Understanding the role of KatG in the INH activation process was hampered by a lack of knowledge of the actual drug binding site. In the plant peroxidases cytochrome *c* peroxidase (CCP) and acorbate peroxidase (APX), with similar but more open heme cavities, INH binds close to the heme *δ*-edge, similarly to other small substrates.[14] This was consistent with the assumption that the peroxidase reaction has a role in INH activation, although it has been shown that it is not essential.[13,15] A binding site for INH and a different one for NAD^+ away from the heme were eventually identified in crystal structures of KatG from *Burkholderia pseudomallei* (BpKatG), which presents the same behavior as MtKatG with respect to INH.[16] The INH binding site found was at the bottom of a small funnel-shaped channel remote from the heme entrance. However, mutations in residues involved in INH binding had

Received: December 17, 2013
Revised: February 24, 2014
Published: February 26, 2014

   dx.doi.org/10.1021/jp4123425 | *J. Phys. Chem. B* 2014, 118, 2924−2931

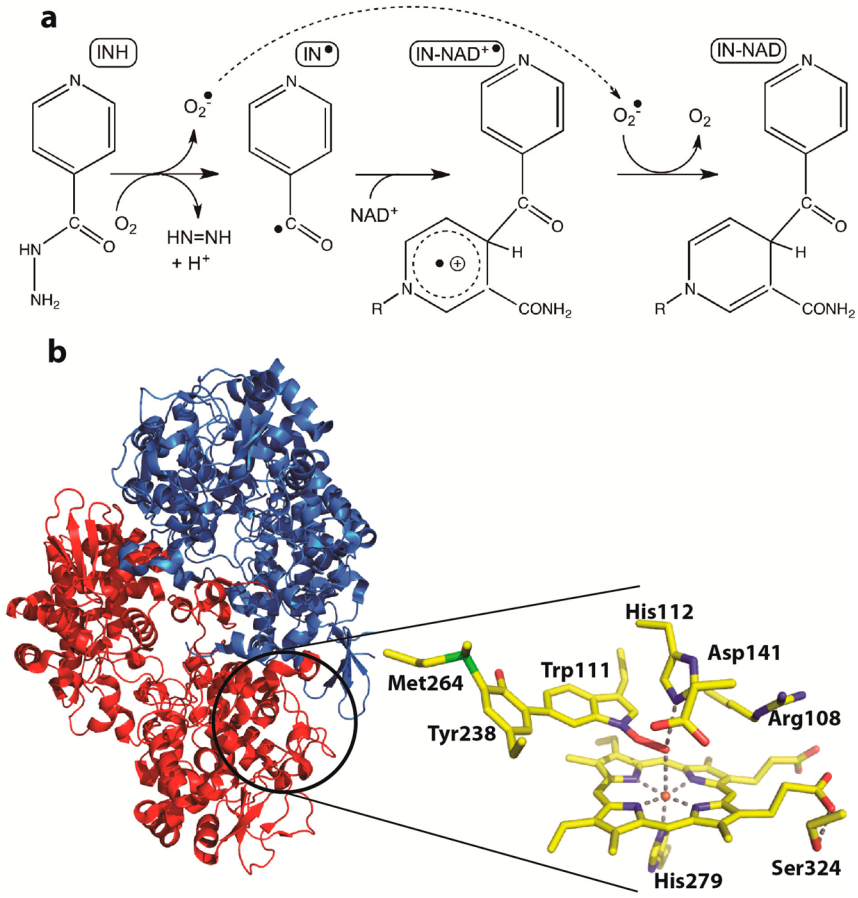

Figure 1. (a) Conversion of INH into IN-NAD involving superoxide.[9] (b) Catalase-peroxidase (KatG), based on the crystal structure of BpKatG (PDB code 2FXJ). The heme and the main active site residues, including the M−Y−W adduct with the frequently found W−OOH modification,[35] are highlighted.

no effect on INH activation, leading to the conclusion that this remote site was not the only binding site for INH.

The binding of INH in the heme cavity of CCP and APX provided a tantalizing suggestion for an alternative INH binding site in KatGs, an idea supported by optical and calorimetric data from KatG.[17] However, binding in the heme cavity of KatGs appears to be complicated by the more constricted entrance to the cavity compared to the wide access channels of CCP and APX. The channel in KatG has a pronounced funnel shape leading to the narrowest section about 8 Å from the heme iron atom, near the side chains of the fully conserved residues in KatGs Asp141 and Ser324 (BpKatG numbering, Figure 1b). Ser324 in BpKatG corresponds to Ser315 in MtKatG, the site with the greatest abundance of mutations imparting INH resistance.[8]

In this work, we investigate, by a combination of molecular dynamics simulations and enhanced sampling methods, the binding of INH in the heme access channel and cavity of BpKatG. The calculations show that INH enters the access channel, but that complete entrance to the heme cavity is restricted by the side chain of Asp141 (Figure 1). Consistently, removal of the carboxylate group in the D141A variant led to the first X-ray crystallography evidence of INH entering the heme cavity.

METHODS

Modeling of INH Binding. Classical molecular dynamics simulations were performed to investigate INH binding in the heme access channel and cavity of ferric KatG. The initial positions of INH were modeled based on their positions in CCP and APX (see Section 1 of the Supporting Information).[14] MD simulations were also performed for the APX:INH and CCP:INH complexes in order to probe the ability of our computational setup to reproduce the X-ray structures (Section 2 of the Supporting Information).

The simulations were performed with the NAMD code,[18] using the AMBER[19,20] (version 99) and TIP3P[21] force fields for protein and water, respectively. Parameters for residues INH, the MYT adduct, and ferric heme were derived according to standard procedures and are reported in Section 3 of the Supporting Information. Simulations performed are at constant temperature and pressure under periodic boundary conditions. Long-range electrostatic interactions were treated with the PME method.[22] A 12 Å cutoff for the real part of the electrostatic and for van der Waals interactions was used.

The metadynamics[23] (MTD) method was used to improve the sampling of conformational space and to reconstruct the free energy surface (FES) for the binding of INH. Metadynamics is a well-assessed technique for sampling the free-energy surface as a function of a few degrees of freedom (collective variables, CVs) via molecular dynamics. It has been previously applied with success to model a number of biological

dx.doi.org/10.1021/jp4123425 | J. Phys. Chem. B 2014, 118, 2924−2931

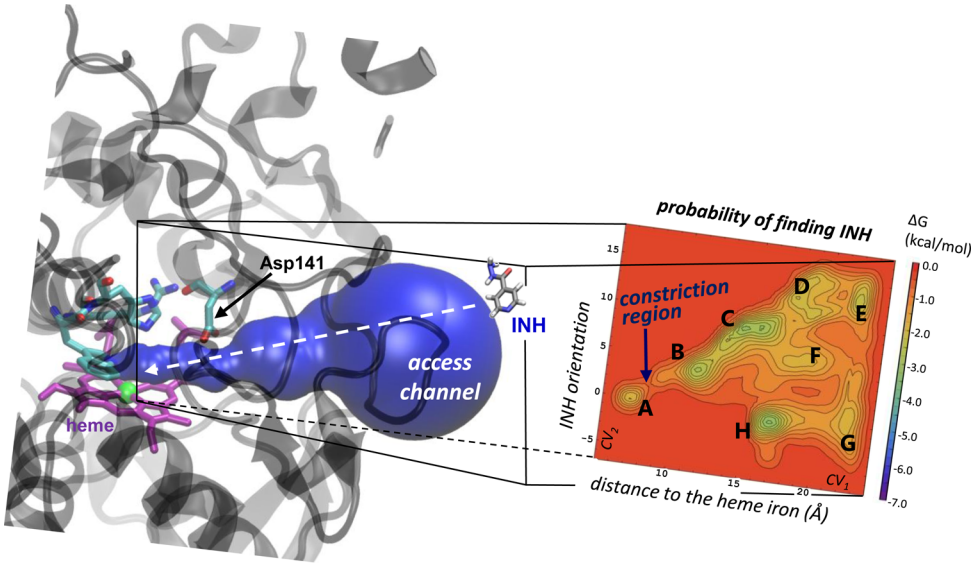

Figure 2. Funnel shape-like access channel of KatG and free energy landscape corresponding to the INH binding to the channel (see collective variable definition in the Supporting Information). Contour lines are separated by 0.25 kcal/mol. The minima of the free energy landscape (labeled A−H) corresponds to the most likely INH binding sites.

processes, including ligand binding to proteins.[24−28] To describe the binding, we used two CVs (see Figure S5 of the Supporting Information): CV_1 was the distance of the ligand (center of mass) from the heme (center of mass); CV_2 was the projection onto the *y* axis of the vector joining the ligand and the heme iron, which provides the position of the ligand along the lateral dimension of the channel. A third variable, the projection of the distance vector onto the *z* axis (CV_3), describing the vertical dimension of the channel, was not included in the metadynamics biasing potential to maintain the computational cost reasonable, but its value was monitored through the simulation. Bounding restraints were applied in order to keep CV_1 and CV_2 within the heme channel ($0 < CV_1 < 22$ Å, $-5 < CV_2 < 15$ Å). The MTD run was initialized from the last snapshot of an equilibrium MD and was performed using the collective variables module implemented in NAMD 2.7. The reconstruction of the free energy surface (FES) was performed by inserting Gaussian biasing potentials of 0.01 kcal/mol height and width 0.2 Å (CV_1) and 0.3 Å (CV_2) every 1000 MD steps. The run was considered converged after 200 ns (details in this respect are given in Section 4 of the Supporting Information). As shown in the Supporting Information, the biasing potential did not alter the structure of the binding site and the reconstructed free energy profile provides a reliable estimate of the binding energetics.

Variant Protein Construction, Purification, and Characterization. The following oligonucleotides were purchased from Invitrogen and used to mutate pBpG-KC containing the *Kpn*I-*Cla*I fragment (base pairs 1−1200) of Bp*katG* or the pBp-CH containing the *Cla*I-*Hin*dIII fragment (base pairs 1003−1731)[29] following the Kunkel procedure:[30]

CCCGACAACGTGAACCTCGAC (A143 V) CCCGACAACCAGAACCTCGAC (A143Q) GCGGGGCCCTACTCGAACGTC (A290Y) GCGGGGCCCCAGTCGAACGTC (A290Q) GTGAATCCGCAAGGCCCGGAC (E242Q) GCCGCCGTGGAGATGGGCCTC (Q233E) AAGATCTGGGACGAACTGAGC (L209D)

CAGATGGGCGACATCTACGTG (L236D) GGCCTCGGCTTCAAGAGCGCG (W309F)

The mutated sequences were confirmed[31] and used to generate the plasmids pA143 V, pA143Q, pA290Y, pA290Q, pE242Q, pQ233E, pL209D, pL236D, and W309F, by reincorporating the fragment into the full-length *katG* gene. The plasmids pD141A and pD141E had been constructed previously.[32] The native and variant proteins were expressed and purified as described.[29] All of the variants except D141A exhibited unchanged catalase and peroxidase activities compared to wild type BpKatG. Catalase activity was determined by the method of Rørth and Jensen[33] in a Gilson oxygraph equipped with a Clark electrode. One unit of catalase is defined as the amount that decomposes 1 μmol of H_2O_2 in 1 min in a 60 μM H_2O_2 solution at pH 7.0 and 37 °C. The synthesis of IN-NAD was assayed by the increase in absorbance at 326 nm (ε = 6900 M^{-1} cm^{-1})[34] of a solution containing 0.4 mM NAD^+, 1.0 mM INH, 2 μM $MnCl_2$, and 50 mM Tris-HCl pH 8.0 at 37 °C. The release of radicals from INH was assayed by the increase in absorbance at 560 nm caused by nitroblue tetrazolium (NBT) reduction to formazan (ε = 18500 M^{-1} cm^{-1}) in a solution containing 1.0 mM INH and 0.2 mM NBT in 50 mM Tris-HCl pH 8.0 at 37 °C.[35] Protein was estimated according to the methods outlined by Layne.[36]

Crystallization and Structure Determination. Crystals of the D141A variant of BpKatG were obtained at 22 °C using the hanging drop vapor diffusion method over a reservoir solution containing 16−20% PEG 4000 (w/v), 20% 2-methyl-2,4-pentanediol (MPD), and 0.1 M sodium citrate pH 5.6.[13,37] Crystals were primitive orthorhombic space group $P2_12_12_1$ with one dimeric molecule in the crystal asymmetric unit. Data sets were collected from crystals flash cooled in the reservoir buffer using synchrotron beamline CMCF 08ID-1 at the Canadian Light Source (CLS) and XALOC beamline at ALBA synchrotron (Cerdanyola del Vallès, Spain). Diffraction data were processed and scaled using programs MOSFLM and SCALA,[38] respectively (Table 2). Structure refinement starting with native BpKatG structure (1MWV) was completed using program REFMAC[39] and manual modeling with the molecular graphics program COOT.[40] Figures were generated using

dx.doi.org/10.1021/jp4123425 | J. Phys. Chem. B 2014, 118, 2924−2931

PYMOL (The PYMOL Molecular Graphics System, Schrödinger, LLC) and VMD.[13]

RESULTS

MD Simulation of INH Binding to Native KatG. The initial positions for INH in the active site of KatG were taken from the X-ray structure of INH complexes with plant peroxidases CCP and APX (see Methods). Two models were generated, CCP-like and APX-like, respectively, and simulations revealed INH binding in both CCP and APX orientations (Figure S4 of the Supporting Information), albeit with a small movement of the Asp141 side chain. However, INH in the APX orientation broke the interaction with Val239 (Figure S4 of the Supporting Information) in the early stages of the simulation (~200 ps), leaving only the CCP-like orientation as being stable within the timescale of the equilibrium MD simulation (3 ns) and a possible model for INH binding to KatG.

Starting from the CCP-like binding site (Figure S1 of the Supporting Information, top panel), a metadynamics simulation was undertaken to find other possible binding sites for INH within the heme access channel (Figure 2). Given the large area to explore (extending up to 22 Å from the heme iron), a long metadynamics simulation (200 ns) was necessary to converge the free energy landscape (Figure 2, right). The results show that INH is accommodated at several binding sites (labeled **A** to **H** in Figure 2) along the heme access channel. Detailed descriptions for all sites are provided in the Supporting Information. All binding sites exhibit a similar rather low binding energy (approximately −2 kcal/mol), making them similarly probable, but weak, binding sites. Binding site **A** (Figure 3) corresponds to the initial CCP-like binding site.

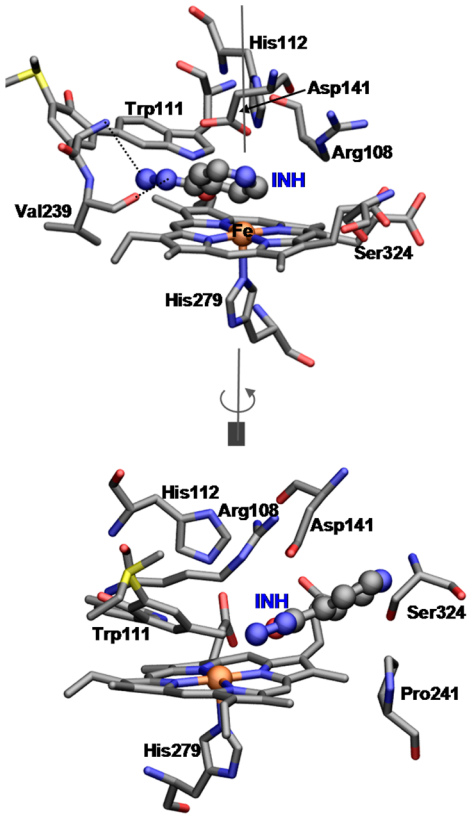

Figure 3. Structure of INH bound at the heme δ-edge obtained from the metadynamics simulation (binding site **A** in Figure 2).

However, accessing spot **A** from **B** requires that a free energy barrier of 2.25 kcal/mol be overcome, corresponding to the passage through a constricted region, which is due to the carboxylate of Asp141 (Figure 2). This result suggested that mutation of D141 to a smaller residue might facilitate the INH access to this site, and this hypothesis was investigated experimentally.

Functional Analysis of INH Binding. To probe the findings of the modeling study and assess the functional roles of the potential INH binding sites in the heme access channel, a number of variants in the binding sites and adjacent sites (as controls) were constructed and their rates of radical generation and IN-NAD synthesis determined (Table 1). Like variants constructed in the previously identified INH binding site, no significant changes compared to the wild-type enzyme are evident in either radical production or IN-NAD synthesis. However, the D141A variant exhibits a 60% higher rate of IN-NAD synthesis (Table 1).

Table 1. Rates of IN-NAD Synthesis

enzyme	IN-NAD[a] (nmol/min)	radical[a]
BpKatG	1.96 ± 0.14	1.08 ± 0.04
D141E	1.75 ± 0.10	0.93 ± 0.02
D141A	3.10 ± 0.17	1.00 ± 0.04
R108A/D141A	2.12 ± 0.09	0.71 ± 0.06
R108A	0.75 ± 0.06	0.69 ± 0.05
A143 V	1.63 ± 0.12	0.85 ± 0.02
A143Q	1.90 ± 0.12	1.10 ± 0.02
A290Y	1.56 ± 0.14	0.58 ± 0.04
A290Q	1.90 ± 0.12	0.74 ± 0.04
S324T	0.92 ± 0.17[b]	0.59 ± 0.09[b]

[a]0.625 μM BpKatG or the variants were used for the IN-NAD assays, and 1.25 μM was used for the radical assays. [b]From ref 9.

If INH was entering the heme cavity and undergoing reaction, it seemed probable that it would interfere with H_2O_2 binding and inhibit the catalatic reaction. Therefore, the effect on catalase activity of INH and its structural analogue benxhydroxamic acid (BHA) was investigated (Figure 4). INH caused less than 5% inhibition of the native enzyme, but as the entrance to the heme cavity was progressively opened in the R108A, D141A, and D141A/R108A variants, progressively greater inhibition was observed. Benzhydroxamic acid caused somewhat greater inhibition in all variants, including the native enzyme and the slightly smaller *p*-, *o*- and *m*-anisidine, like *o*-dianisidine,[41] caused even greater inhibition in the order *p*- > *o*- > *m*- (Figure S18 of the Supporting Information). The peroxidatic reaction was not tested because of reaction of the isonicotinyl radicals with peroxidatically formed ABTS radicals. These results show that, as predicted by the metadynamics simulations, the carboxylate group of Asp141 constricts the entrance of INH to the active site.

Crystal Structure of D141A in Complex with INH. Crystals of D141A were grown under similar conditions as in our previous study in which an INH binding site was identified in a remote site (0, 5, and 100 mM INH, Table 2).[13] The region of electron density corresponding to INH bound near Glu198 was evident in maps from crystals grown with both 5 and 100 mM INH, but the maps of the 100 mM crystals contained in addition a region of strong electron density in the heme cavity that corresponded well with the structure of INH and suggested high occupancy at the site (Figure 5). In light of

dx.doi.org/10.1021/jp4123425 | J. Phys. Chem. B 2014, 118, 2924−2931

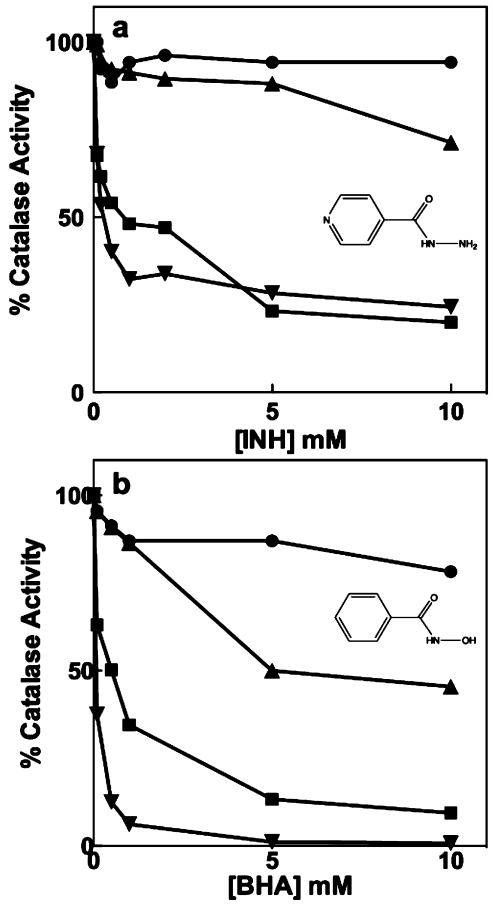

Figure 4. Effect of (a) INH and (b) benzhydroxamic acid on the catalase activity of wild-type BpKatG (●), R108A (▲), D141A (■), and R108A/D141A (▼).

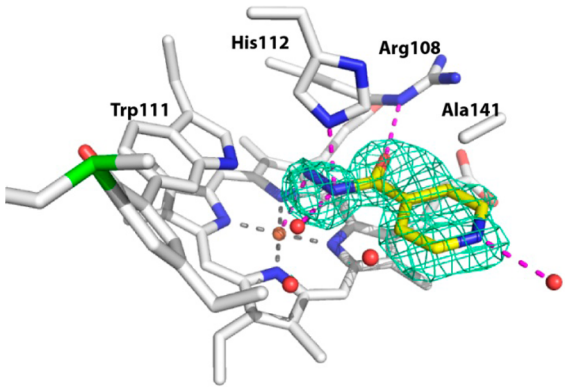

Figure 5. Active center of the D141A variant of BpKatG, with the *Fo*−*Fc* electron density map calculated without INH in the model and drawn at σ = 3 with INH superimposed. Interactions between INH and the adjacent waters, side chains, and heme iron are indicated with dashed lines in magenta.

this result, crystals of wild-type BpKatG were grown in the presence of 100 mM INH, to see if INH could be forced into the heme cavity, but no additional electron density was evident in the heme cavity compared with the crystals grown without and with 5 mM INH.[13] This again confirmed the barrier to INH entry into the heme cavity of wild-type KatGs. The structure of D141A without INH present differed from the wild-type enzyme only in the vicinity of the missing carboxylate group. Occupancy of INH in the heme cavity of D141A could also be achieved by soaking but an even higher concentration (300 mM) was required (Table 2).

Table 2. Data Collection and Refinement Statistics

(A) data collection statistics		
sample	D141A-INH (cocrystal)	D141A-INH (soaked)
PDB	4KA6	4KWQ
Unit cell		
a (Å)	100.77	100.64
b (Å)	115.59	114.64
c (Å)	174.57	174.99
α, β, γ (deg)	90.0	90.0
resolution[a]	41.0−1.70 (1.79−1.70)	48.0−1.88 (1.97−1.87)
unique reflections	222093 (32036)	163289 (22743)
completeness %	99.5 (99.2)	98.3 (95.1)
R_{merge}	0.089 (0.403)	0.085 (0.492)
$\langle I/\sigma I \rangle$	10.7 (3.2)	14.3 (2.1)
multiplicity	5.1 (4.8)	3.6 (3.2)
(B) model refinement statistics		
no. reflections	210857	155033
R_{cryst} (%)	15.9	15.3
R_{free} (%)	17.9	18.1
non-H atoms	11155	11340
water molecules	1068	1073
average B-factor Å^2		
protein	22.1	20.9
heme	15.8	15.5
waters	27.8	33.8
other		
Coor. error (Å)[b]	0.050	0.065
rms dev. bonds (Å)	0.023	0.019
rms dev. angles (deg)	2.06	1.79

[a]Values in parentheses correspond to the highest-resolution shell. [b]Based on maximum likelihood.

The location of INH deep in the heme cavity of D141A differs from its location in CCP and APX. The terminal $-NH_2$ (N_3) of INH is situated 2.4 Å above the heme iron and the C═O of INH is situated 2.7 Å from N_ε of the catalytic Arg108. Both N_3 and N_2 of INH (NH_2 and NH, respectively) are within hydrogen-bonding distance (2.6−3.1 Å) of the imidazole $N_{\varepsilon 2}$ of the catalytic His112 (Figure 5), albeit with less-than-ideal geometry for hydrogen bond formation. Other INH interactions include a 2.8 Å hydrogen bond between N_2 (NH) and the first of a string of three water molecules in the heme cavity and a 2.7 Å hydrogen bond between N_1 and a water in the channel. The pyridine ring of INH projects out of the cavity into the entrance channel with its C_1 located between the heme methyl group (3.8 Å) and the Ala141 methyl group (4.5 Å).

The obstruction to INH entry to the heme cavity created by the D141 carboxylate becomes clear when the binding location of INH in D141A is superimposed into the wild-type structure (Figure 6). The conflicts between the pyridine ring and the carboxylate involve distances of less than 2.1 Å. The entrance to the heme cavity of the S324T variant (equivalent to S315T in MtKatG) where the additional methyl group creates additional conflicts with INH is even more restricted.[42]

dx.doi.org/10.1021/jp4123425 | J. Phys. Chem. B 2014, 118, 2924−2931

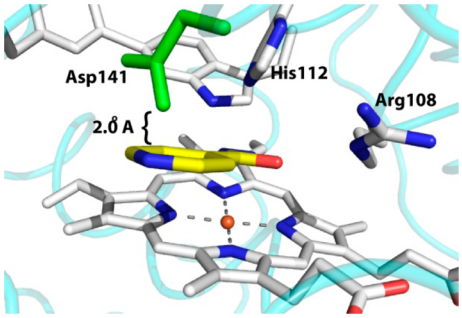

Figure 6. Superposition of INH as bound in D141A into the heme cavity of wild-type BpKatG. Distances marked by red dashes between the closest atoms of INH molecule and the adjacent carboxylate of Asp141 (shown in green) illustrate the steric conflicts that would interfere with INH binding at this site.

DISCUSSION

The binding site of the antitubercular pro-drug INH in KatG remains a subject of debate. Whereas binding in the heme pocket has been proposed by several studies,[14,17,43] structural characterization of INH in this region has proven to be elusive. In this work, we have investigated the binding of INH in the access channel of KatG with a combination of molecular dynamics, X-ray crystallography, and site-directed mutagenesis.

Molecular dynamics simulations were performed taking full account of protein flexibility, in combination with an enhanced sampling technique (metadynamics). Three main conclusions can be extracted from the analysis of the free-energy landscape of INH binding (Figure 2). First, there are several weak INH binding sites along the access channel. Second, INH binding at the heme-δ edge, but not deep in the heme cavity, as proposed based on the X-ray structures of INH in complex with the homologous class I peroxidase CCP, leads to stable binding (site A in Figure 2) in both the ferric and Cpd I states. However, third, access to site A is restricted by the reduced size of the heme access channel compared to plant peroxidases caused by the side chain of Asp141. The carboxylate group extends into the heme channel and shows little flexibility, being anchored by an H-bond to backbone NH of Ile237. This structural determinant is reflected in the free-energy landscape, showing that moving to (and out from) site A requires the passage through higher-energy conformations.

Interestingly, the crystal structure of the INH-resistant mutant S324T (S315T in MtKatG)[42] showed that the side chain methyl group is situated in the entrance channel and thus would further narrow the access to the heme. Activity experiments revealed that the mutant maintains normal catalase and peroxidase activities, whereas IN-NAD synthase was reduced. Other authors reported on the reduced affinity of the MtKatG S315T mutant for INH.[8] This result is in line with our findings (S324T would make difficult the access to site **B** from **C**), suggesting that an even higher barrier would be encountered by INH on its way to the heme distal cavity in the case of the bulkier substituent.

The observation that Asp141 restricts the access of INH to the heme active site prompted us to hypothesize that removing the constriction would facilitate INH entrance to the heme distal pocket. In fact, characterization of the D141A variant confirms that removal of the D141 carboxylate did indeed enhance access of INH to the heme distal pocket. For example, INH caused substantial inhibition of the catalatic reaction of D141A, whereas it had little or no effect on the wild-type BpKatG reaction. However, more convincingly, the D141A-INH crystal structure revealed INH bound in the heme cavity. Interestingly, the INH was situated much deeper in the cavity than in CCP or the equivalent site A in the simulation of wild-type KatG making contact with the heme iron and adjacent catalytic residues. In this location, it would interfere with H_2O_2 binding, readily explaining its inhibition of the catalatic process. Other small aromatic molecules, including the structural analogue BHA and the somewhat smaller anisidine isomers, cause even greater inhibition in both the wild-type enzyme and D141A, suggesting that it is more than a simple size or shape criterion that lowers INH accessibility.

It is to be noted that the binding mode of INH in the D141A mutant is different from what was predicted for the wild-type enzyme (Figure 3). In the X-ray structure, INH sits on top of the heme group, with the carbonyl group involved in a hydrogen bond interaction with both the side chain of Arg108 and the terminal N of the hydrazine group that in turn interacts with the iron atom (Figure 5). The latter interaction is not properly reproduced by the molecular mechanics interaction potential in the model of wild-type BpKatG, explaining why this binding mode was not observed during the MD simulation.

Significantly, even in the more open heme cavity of D141A, the binding affinity of INH remains weak. This is reflected in the incomplete inhibition of the catalase reaction caused by INH (Figure 4a) and the high concentrations of INH, 100 mM for cocrystallization and 300 mM for soaking, required to reach high occupancy in the crystal structures. For comparison, only 0.63 mM INH is used in the standard assays for IN-NAD synthesis and 5 mM INH yields high occupancy binding near Glu198.

In summary, the suggestion of a number of weak binding sites in the heme entrance channel together with the INH binding site previously found remote from the heme near Glu198[13] makes it clear that there are several weak INH binding sites in KatGs. This may explain why attempts to observe INH by cocrystallization or soaking had little success so far. Interestingly, our results are consistent with the results of a recent study[44] showing that the D141Ser mutant exhibits a significant increase of IN-NAD synthesis. It was suggested that such activity increase was due to a larger access channel. Here, we provided detailed structural and computational evidence of INH entering the access channel in the D141A mutant. Overall, these observations contribute to an advance in our understanding of how the pro-drug INH is activated by KatG. Furthermore, the results suggest that the effectiveness of a drug may depend not only on its binding affinity but also on how easily it may access the binding site. In this respect, the techniques used here, which do not assume any prior knowledge of the binding site's location within a given region of the protein, may contribute insight to facilitate the design of potent inhibitors.[24,45]

ASSOCIATED CONTENT

Supporting Information

Further details of the calculations and inhibition data. This material is available free of charge via the Internet at http://pubs.acs.org.

dx.doi.org/10.1021/jp4123425 | J. Phys. Chem. B 2014, 118, 2924−2931

AUTHOR INFORMATION

Corresponding Author

*E-mail: c.rovira@ub.edu. Tel: +34 93 4039254. Fax: +34 93 3397878.

Author Contributions

○P.V. and P.C.L. contributed equally.

Notes

The authors declare no competing financial interest.

ACKNOWLEDGMENTS

Financial support was provided by MINECO (Grants CTQ2011-25871 and BFU2012-36827), GENCAT (Grant 2009SGR-1309), NSERC (Discovery Grant 9600), and the Canada Research Chair Program (to P.C.L.). We acknowledge the computer support, technical expertise, and assistance provided by the Barcelona Supercomputing Center-Centro Nacional de Supercomputación (BSC-CNS). We thank J. Iglesias-Fernández for technical assistance.

REFERENCES

(1) Zhang, Y.; Heym, B.; Allen, B.; Young, D.; Cole, S. The Catalase-Peroxidase Gene and Isoniazid Resistance of Mycobacterium Tuberculosis. *Nature* **1992**, *358*, 591−593.

(2) Njuma, O. J.; Ndontsa, E. N.; Goodwin, D. C. Catalase in Peroxidase Clothing: Interdependent Cooperation of Two Cofactors in the Catalytic Versatility of KatG. *Arch. Biochem. Biophys.* **2013**, *544*, 27−39.

(3) Wakamoto, Y.; Dhar, N.; Chait, R.; Schneider, K.; Signorino-Gelo, F.; Leibler, S.; McKinney, J. D. Dynamic persistence of antibiotic-stressed mycobacteria. *Science* **2013**, *339*, 91−95.

(4) Cade, C. E.; Dlouhy, A. C.; Medzihradszky, K. F.; Salas-Castillo, S. P.; Ghiladi, R. A. Isioniazid-Resistance Conferring Mutations in Mycobacterium Tuberculosis KatG: Catalase, Peroxidase, and INH-NADH Adduct Formation Activities. *Protein Sci.* **2010**, *19*, 458−474.

(5) Rouse, D. A.; DeVito, J. A.; Li, Z. M.; Byer, H.; Morris, S. L. Site-Directed Mutagenesis of the KatG Gene of Mycobacterium Tuberculosis: Effects on Catalase-Peroxidase Activities and Isoniazid Resistance. *Mol. Microbiol.* **1996**, *22*, 583−592.

(6) Saint-Joanis, B.; Souchon, H.; Wilming, M.; Johnsson, K.; Alzari, P. M.; Cole, S. T. Use of Site-Directed Mutagenesis to Probe the Structure, Function and Isoniazid Activation of the Catalase/Peroxidase, KatG, from Mycobacterium Tuberculosis. *Biochem. J.* **1999**, *338*, 753−760.

(7) Rattan, A.; Kalia, A.; Ahmad, N. Multidrug-Resistant Mycobacterium Tuberculosis: Molecular Perspectives. *Emerging Infect. Dis.* **1998**, *4*, 195−209.

(8) Yu, S.; Girotto, S.; Lee, C.; Magliozzo, R. S. Reduced Affinity for Isoniazid in the S315T Mutant of Mycobacterium Tuberculosis KatG is a Key Factor in Antibiotic Resistance. *J. Biol. Chem.* **2003**, *278*, 14769−14775.

(9) Heym, B.; Alzari, P. M.; Honore, N.; Cole, S. T. Missense Mutations in the Catalase-Peroxidase Gene, katG, are Associated with Isoniazid Resistance in Mycobacterium Tuberculosis. *Mol. Microbiol.* **1995**, *15*, 235−245.

(10) Wilming, M.; Johnsson, K. Spontaneous Formation of the Bioactive Form of the Tuberculosis Drug Isoniazid. *Angew. Chem., Int. Ed. Engl.* **1999**, *38*, 2588−2590.

(11) Rozwarski, D. A.; Grant, G. A.; Barton, D. H. R.; Jacobs, W. R.; Sacchettini, J. C. Modification of the NADH of the Isoniazid Target (InhA) from Mycobacterium Tuberculosis. *Science* **1998**, *279*, 98−102.

(12) Timmins, G. S.; Deretic, V. Mechanisms of Action of Isoniazid. *Mol. Microbiol.* **2006**, *62*, 1220−1227.

(13) Wiseman, B.; Carpena, X.; Feliz, M.; Donald, L. J.; Pons, M.; Fita, I.; Loewen, P. C. Isonicotinic Acid Hydrazide Conversion to Isonicotinyl-NAD by Catalase-Peroxidases. *J. Biol. Chem.* **2010**, *285*, 26662−26673.

(14) Metcalfe, C.; Macdonald, I. K.; Murphy, E. J.; Brown, K. A.; Raven, E. L.; Moody, P. C. E. The Tuberculosis Prodrug Isoniazid Bound to Activating Peroxidases. *J. Biol. Chem.* **2008**, *283*, 6193−6200.

(15) Wengenack, N. L.; Hoard, H. M.; Rusnak, F. Isoniazid oxidation by Mycobacterium tuberculosis KatG: A Role for Superoxide which Correlates with Isoniazid Susceptibility. *J. Am. Chem. Soc.* **1999**, *121*, 9748−9749.

(16) Singh, R.; Wiseman, B.; Deemagarn, T.; Jha, V.; Switala, J.; Loewen, P. C. Comparative Study of Catalase-Peroxidases (KatGs). *Arch. Biochem. Biophys.* **2008**, *471*, 207−214.

(17) Zhao, X.; Yu, S.; Magliozzo, R. S. Characterization of the Binding of Isoniazid and Analogues to Mycobacterium Tuberculosis Catalase-Peroxidase. *Biochemistry* **2007**, *46*, 3161−3170.

(18) Phillips, J. C.; Braun, R.; Wang, W.; Gumbart, J.; Tajkhorshid, E.; Villa, E.; Chipot, C.; Skeel, R. D.; Kale, L.; Schulten, K. Scalable Molecular Dynamics with NAMD. *J. Comput. Chem.* **2005**, *26*, 1781−1802.

(19) Cornell, W. D.; Cieplak, P.; Bayly, C. I.; Gould, I. R.; Merz, K. M.; Ferguson, D. M.; Spellmeyer, D. C.; Fox, T.; Caldwell, J. W.; Kollman, P. A. A 2nd Generation Force-Field for the Simulation of Proteins, Nucleic Acids, and Organic Molecules. *J. Am. Chem. Soc.* **1995**, *117*, 5179−5197.

(20) Cheatham, T. E.; Cieplak, P.; Kollman, P. A. A modified Version of the Cornell et al. Force Field with Improved Sugar Pucker Phases and Helical Repeat. *J. Biomol. Struct. Dyn.* **1999**, *16*, 845−862.

(21) Jorgensen, W. L.; Chandrasekhar, J.; Madura, J. D.; Impey, R. W.; Klein, M. L. Comparison of Simple Potential Functions for Simulating Liquid Water. *J. Chem. Phys.* **1983**, *79*, 926−935.

(22) Essmann, U.; Perera, L.; Berkowitz, M. L.; Darden, T.; Lee, H.; Pedersen, L. G. A Smooth Particle Mesh Ewald Method. *J .Chem. Phys.* **1995**, *103*, 8577−8593.

(23) Laio, A.; Parrinello, M. Escaping Free-Energy Minima. *Proc. Natl. Acad. Sci. U.S.A.* **2002**, *99*, 12562−12566.

(24) Gervasio, F. L.; Laio, A.; Parrinello, M. Flexible Docking in Solution Using Metadynamics. *J. Am. Chem. Soc.* **2005**, *127*, 2600−2607.

(25) Limongelli, V.; Bonomi, M.; Marinelli, L.; Gervasio, F. L.; Cavalli, A.; Novellino, E.; Parrinello, M. Molecular Basis of Cyclooxygenase Enzymes (COXs) Selective Inhibition. *Proc. Natl. Acad. Sci. U.S.A.* **2010**, *107*, 5411−5416.

(26) Biarnes, X.; Bongarzone, S.; Vargiu, A. V.; Carloni, P.; Ruggerone, P. Molecular Motions in Drug Design: The Coming Age of the Metadynamics Method. *J. Comput.-Aided Mol. Des.* **2011**, *25*, 395−402.

(27) Henin, J.; Fiorin, G.; Chipot, C.; Klein, M. L. Exploring Multidimensional Free Energy Landscapes Using Time-Dependent Biases on Collective Variables. *J. Chem. Theory Comput.* **2010**, *6*, 35−47.

(28) Fiorin, G.; Klein, M. L.; Hénin, J. Using Collective Variables to Drive Molecular Dynamics Simulations. *Mol. Phys.* **2013**, *111*, 3345−3362.

(29) Colin, J.; Wiseman, B.; Switala, J.; Loewen, P. C.; Ivancich, A. Distinct Role of Specific Tryptophans in Facilitating Electron Transfer or as [Fe(IV)═O Trp(*)] Intermediates in the Peroxidase Reaction of Bulkholderia Pseudomallei Catalase-Peroxidase: A Multifrequency EPR Spectroscopy Investigation. *J. Am. Chem. Soc.* **2009**, *131*, 8557−8563.

(30) Kunkel, T. A.; Roberts, J. D.; Zakour, R. A. Rapid and Efficient Site-Specific Mutagenesis without Phenotypic Selection. *Methods Enzymol.* **1987**, *154*, 367−382.

(31) Sanger, F.; Nicklen, S.; Coulson, A. R. DNA Sequencing with Chain-Terminating Inhibitors. *Proc. Natl. Acad. Sci. U.S.A.* **1977**, *74*, 5463−5467.

(32) Deemagarn, T.; Wiseman, B.; Carpena, X.; Ivancich, A.; Fita, I.; Loewen, P. C. Two Alternative Substrate Paths for Compound I Formation and Reduction in Catalase-Peroxidase KatG from Burkholderia Pseudomallei. *Proteins* **2007**, *66*, 219−228.

(33) Rorth, M.; Jensen, P. K. Determination of Catalase Activity by means of the Clark Oxygen Electrode. *Biochim. Biophys. Acta* **1967**, *139*, 171−173.
(34) Rawat, R.; Whitty, A.; Tonge, P. J. The Isoniazid-NAD Adduct is a Slow, Tight-Binding Inhibitor of InhA, the Mycobacterium tuberculosis Enoyl Reductase: Adduct Affinity and Drug Resistance. *Proc. Natl. Acad. Sci. U.S.A.* **2003**, *100*, 13881−13886.
(35) Auclair, C.; Torres, M.; Hakim, J. Superoxide Anion Involvement in NBT Reduction Catalyzed by NADPH-Cytochrome P-450 Reductase: A Pitfall. *FEBS Lett.* **1978**, *89*, 26−28.
(36) Layne, E. *Methods Enzymol.* **1957**, *3*, 447−454.
(37) Carpena, X.; Loprasert, S.; Mongkolsuk, S.; Switala, J.; Loewen, P. C.; Fita, I. Catalase-Peroxidase KatG of Burkholderia Pseudomallei at 1.7A Resolution. *J. Mol. Biol.* **2003**, *327*, 475−489.
(38) Collaborative Computational Project, N. The CCP4 Suite: Programs for Protein Crystallography. *Acta Crystallogr.* **1994**, *D50*, 760−763.
(39) Murshudov, G. N.; Vagin, A. A.; Dodson, E. J. Refinement of Macromolecular Structures by the Maximum-Likelihood Method. *Acta Crystallogr., Sect. D: Biol. Crystallogr.* **1997**, *53*, 240−255.
(40) Emsley, P.; Cowtan, K. Coot: Model-Building Tools for Molecular Graphics. *Acta Crystallogr., Sect. D: Biol. Crystallogr.* **2004**, *60*, 2126−2132.
(41) Claiborne, A.; Fridovich, I. Purification of the o-Dianisidine Peroxidase from Escherichia Coli B. Physicochemical Characterization and Analysis of its Dual Catalatic and Peroxidatic Activities. *J. Biol. Chem.* **1979**, *254*, 4245−4252.
(42) Deemagarn, T.; Carpena, X.; Singh, R.; Wiseman, B.; Fita, I.; Loewen, P. C. Structural Characterization of the Ser324Thr Variant of the Catalase-Peroxidase (KatG) from Burkholderia Pseudomallei. *J. Mol. Biol.* **2005**, *345*, 21−28.
(43) Pierattelli, R.; Banci, L.; Eady, N. A.; Bodiguel, J.; Jones, J. N.; Moody, P. C.; Raven, E. L.; Jamart-Gregoire, B.; Brown, K. A. Enzyme-Catalyzed Mechanism of Isoniazid Activation in Class I and Class III Peroxidases. *J. Biol. Chem.* **2004**, *279*, 39000−39009.
(44) Zhao, X.; Hersleth, H. P.; Zhu, J.; Andersson, K. K.; Magliozzo, R. S. Access Channel Residues Ser315 and Asp137 in Mycobacterium Tuberculosis catalase-peroxidase (KatG) Control Peroxidatic Activation of the Pro-Drug Isoniazid. *Chem. Commun.* **2013**, *49*, 11650−11652.
(45) Shan, Y.; Kim, E. T.; Eastwood, M. P.; Dror, R. O.; Seeliger, M. A.; Shaw, D. E. How Does a Drug Molecule Find its Target Binding Site? *J. Am. Chem. Soc.* **2011**, *133*, 9181−9183.